Articles

Intercalation of the (1*S*,2*R*,3*S*,4*R*)-N^6-[1-(1,2,3,4-Tetrahydro-2,3,4-trihydroxybenz[*a*]anthracenyl)]-2′-deoxyadenosyl Adduct in an Oligodeoxynucleotide Containing the Human *N-ras* Codon 61 Sequence†

Zhijun Li, Hye-Young Kim, Pamela J. Tamura, Constance M. Harris, Thomas M. Harris, and Michael P. Stone*

Department of Chemistry and Center in Molecular Toxicology, Vanderbilt University, Nashville, Tennessee 37235

Received February 15, 1999; Revised Manuscript Received August 25, 1999

ABSTRACT: The (1*S*,2*R*,3*S*,4*R*)-N^6-[1-(1,2,3,4-tetrahydro-2,3,4-trihydroxybenz[*a*]anthracenyl)]-2′-deoxyadenosyl adduct at X^6 of 5′-d(CGGACXAGAAG)-3′•5′-d(CTTCTTGTCCG)-3′, incorporating codons 60, 61 (underlined), and 62 of the human *N-ras* protooncogene, results from trans opening of (1*R*,2*S*,3*S*,4*R*)-1,2-epoxy-1,2,3,4-tetrahydrobenz[*a*]anthracenyl-3,4-diol by the exocyclic N^6 of adenine. Two conformations of this adduct exist, in slow exchange on the NMR time scale. A structure for the major conformation, which represents approximately 80% of the population, is presented. In this conformation, an anti glycosidic torsion angle is observed for all nucleotides, including $^{S,R,S,R}A^6$. The refined structure is a right-handed duplex, with the benz[*a*]anthracene moiety intercalated on the 3′-face of the modified base pair, from the major groove. It is located between $^{S,R,S,R}A^6$•T^{17} and A^7•T^{16}. Intercalation is on the opposite face of the modified $^{S,R,S,R}A^6$•T^{17} base pair as compared to the (1*R*,2*S*,3*R*,4*S*)-N^6-[1-(1,2,3,4-tetrahydro-2,3,4-trihydroxybenz[*a*]anthracenyl)]-2′-deoxyadenosyl adduct, which intercalated 5′ to the modified $^{R,S,R,S}A^6$•T^{17} base pair [Li, Z., Mao, H., Kim, H.-Y., Tamura, P. J., Harris, C. M., Harris, T. M., and Stone, M. P. (1999) *Biochemistry 38,* 2969−2981]. The spectroscopic data do not allow refinement of the minor conformation, but suggest that the adenyl moiety in the modified nucleotide $^{S,R,S,R}A^6$ adopts a syn glycosidic torsion angle. Thus, the minor conformation may create greater distortion of the DNA duplex. The results are discussed in the context of site-specific mutagenesis studies which reveal that the $^{S,R,S,R}A^6$ lesion is less mutagenic than the $^{R,S,R,S}A^6$ lesion.

The polycyclic aromatic hydrocarbon (PAH)[1] class of mutagens, which includes benz[*a*]anthracene, has been recognized since the incidence of scrotal cancer in chimney sweeps was linked to occupational exposure to soot (*1*). The genotoxicity of these compounds is generally recognized to result from their stepwise oxidation by cytochromes P_{450} (*2*, *3*), typically to stereoisomeric "bay region" electrophilic diol epoxides. These adduct nucleophilic sites are on the bases of DNA, especially guanine N^2 (*4*−*6*), but also on other sites, including adenine N^6 (*7*, *8*).

Benz[*a*]anthracene (BA) is a significant PAH component of coal tar, atmospheric pollution (*9*, *10*), automobile exhaust, and cigarette smoke (*11*). Of the (+)- and (−)-enantiomers of the diastereomeric bay region BA diol epoxides, (+)-(1*R*,2*S*,3*S*,4*R*)-3,4-dihydroxy-1,2-epoxy-1,2,3,4-tetrahydrobenz-[*a*]anthracene [(+)-DE2] has significant tumor-initiating activity in mouse skin and newborn mice (*12*). This diol epoxide has the same absolute configuration as the highly tumorigenic isomers of the benzo[*a*]pyrene and chrysene bay region diol epoxides. The bay region diol epoxides of BA are also mutagenic in bacterial strains and in V79-6 Chinese hamster lung cells (*13*−*15*). However, BA is somewhat less carcinogenic than benzo[*a*]pyrene or dibenz[*a*,*h*]anthracene (*16*, *17*). The mutagenicity of the bay region diol epoxides suggests that the lower carcinogenicity of BA as compared to those of the other PAHs may be due in part to a lower level of metabolism to the bay region diol epoxide (*18*−*21*).

† This work was supported by NIH Grant ES-05355. Funding for the NMR spectrometer was supplied by NIH Grant RR-05805 and the Vanderbilt Center in Molecular Toxicology (Grant ES-00267). The National Magnetic Resonance Facility at Madison was funded by the University of Wisconsin, NSF Grants DMB-8415048 and BIR-9214394, NIH Grants RR-02301, RR-02781, and RR08438, and the USDA.

* To whom correspondence should be addressed. Phone: (615) 322-2589. Fax: (615) 343-1234. E-mail: stone@toxicology.mc.vanderbilt.edu.

[1] Abbreviations: BADE, benz[*a*]anthracene diol epoxide; BPDE, benzo[*a*]pyrene diol epoxide; EDTA, ethylenediaminetetraacetic acid; HPLC, high-pressure liquid chromatography; NOE, nuclear Overhauser enhancement; NOESY, two-dimensional NOE spectroscopy; PAH, polycyclic aromatic hydrocarbon; ROESY, rotating-frame Overhauser enhancement spectroscopy; TPPI, time-proportional phase increment. A right superscript refers to the numerical position in the sequence starting from the 5′-terminus of chain A and proceeding to the 3′-terminus of chain A, and then from the 5′-terminus of chain B to the 3′-terminus of chain B. C2, C5, C6, C8, C1′, C2′, C2″, etc., represent specific carbon nuclei. H2, H5, H6, H8, H1′, H2′, H2″, etc., represent protons attached to these carbons.

10.1021/bi9903650 CCC: $18.00
Published on Web 11/11/1999

Chart 1: (A) BA SRSR(61,2) Oligodeoxynucleotide, Where X Is the (1*S*,2*R*,3*S*,4*R*)-N^6-[1-(1,2,3,4,-Tetrahydro-2,3,4-trihydroxybenz[*a*]anthracenyl)]-2′-deoxyadenosyl Adduct, and (B) the (1*S*,2*R*,3*S*,4*R*)-N^6-[1-(1,2,3,4,-Tetrahydro-2,3,4-trihydroxybenz[*a*]anthracenyl)]-2′-deoxyadenosyl Adduct and Designations of the Benz[*a*]anthracene Protons

A

ras codons

60 61 62

5′-C^1 | G^2 G^3 A^4 | C^5 X^6 A^7 | G^8 A^9 A^{10} | G^{11}-3′

3′-G^{22} | $C^{21}C^{20}T^{19}$ | $G^{18}T^{17}T^{16}$ | $C^{15}T^{14}T^{13}$ | C^{12}-5′

B

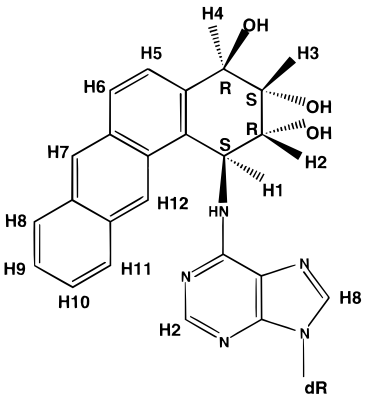

We have used the *ras61* oligodeoxynucleotide 5′-d(CGGACAAGAAG)-3′•5′-d(CTTCTTGTCCG)-3′ as a model (*22*) (Chart 1) to examine the solution conformations of adenyl N^6 α-styrene oxide (*23*−*25*), benzo[*a*]pyrene (*26*) adducts, and a benz[*a*]anthracene adduct (*27*). Mutations within codon 61 cause oncogene activation (*28*). Each of these studies was facilitated by the development of a nonbiomimetic synthesis enabling large-scale production of site-specifically modified oligodeoxynucleotides, while simultaneously eliminating problems in controlling the regioselectivity of adduction (*29*). This method was extended to production of the (1*S*,2*R*,3*S*,4*R*)-N^6-[1-(1,2,3,4-tetrahydro-2,3,4-trihydroxybenz[*a*]anthracenyl)]-2′-deoxyadenosyl adduct (*30*−*32*), at 5′-d(CGGACXAGAAG)-3′•5′-d(CTTCTTGTCCG)-3′, where X is the adducted adenine. This was named the BA SRSR(61,2) adduct (Chart 1).

BA adducts at adenine N^6 are less abundant, as compared to the corresponding guanine N^2 adducts. Nevertheless, the minor adenyl N^6 adducts are of interest because the relation between the major and minor sites of covalent adduction and mutagenesis remains incompletely understood. The possibility exists that the minor adenine lesions may have disproportionate biological significance as has been suggested for adenine N^6 dimethylbenz[*a*]anthracene (*33*), benzo[*a*]pyrene (*34*), and dibenzo[*a*,*l*]pyrene (*35*) adducts. Accordingly, understanding how benzo[*a*]pyrene (*26*, *36*−*39*), benzo[*c*]-phenanthrene (*40*, *41*), and styrene oxide (*23*−*25*) adducts at adenine N^6 alter the conformation of duplex DNA has been of considerable interest (*42*).

BA is activated to both bay and non-bay region diol epoxides (*2*) and thus provides a useful model for understanding PAH structure−activity relationships. Using a repair-deficient prokaryotic in vivo replication system, the bay region adenyl N^6 BA RSRS(61,2) and SRSR(61,2) adducts were observed to be mutagenic, whereas the corresponding non-bay region adducts were not (*43*). Site-specific mutagenesis demonstrated that the adenyl N^6 BA RSRS(61,2) lesion induced A → G transitions, similar to those observed for the adenyl N^6 benzo[*a*]pyrene SRSR(61,2) adduct with corresponding stereochemistry (*44*). The mutagenic frequency was dependent on the stereochemistry about the adduct-forming bond. The BA SRSR(61,2) adduct which is the subject of the work presented here was less mutagenic than the BA RSRS(61,2) adduct. Mutagenic frequency also varied with the strain of *Escherichia coli* in which these adducts were replicated. These adducts blocked replication in vitro by *E. coli* DNA polymerase III holoenzyme (*43*). We reported the solution structure of the BA RSRS(61,2) adduct placed opposite thymine in duplex DNA (*27*). A single conformation was observed, in which the adduct intercalated toward the 5′-direction from the site of adduction, similar to the corresponding adduct of benzo[*a*]pyrene at this location (*26*). Those results were discussed in relation to site-directed mutagenesis studies (*43*, *44*) which revealed similarities in the biological processing of benz[*a*]anthracene and benzo[*a*]pyrene adducts with corresponding stereochemistry. Both of these adducts having (*R*)-stereochemistry at the benzylic carbon yielded A → G mutations (*43*).

We have subsequently focused on the BA SRSR(61,2) adduct, which corresponds to the product arising by adduction of the (1*R*,2*S*,3*S*,4*R*)-3,4-dihydroxy-1,2-epoxy-1,2,3,4-tetrahydrobenz[*a*]anthracene [(+)-DE2] at adenine N^6. Two interchangeable conformations of the SRSR(61,2) adduct are observed, termed the major conformation and the minor conformation. We have refined a solution structure for the major conformation, in which an anti glycosidic torsion angle is observed for all nucleotides, including $^{S,R,S,R}A^6$. Molecular dynamics calculations restrained by ^{1}H nuclear Overhauser effects (*45*, *46*) demonstrate that the anthracenyl moiety intercalates to the 3′-face of the modified adenine from the major groove. It has not been possible to refine the structure of the minor conformation. However, the NOESY data suggest that in the minor conformation the modified dA^6 adopts a syn glycosidic torsion angle. These results differ from those for the BA RSRS(61,2) adduct, which intercalated from the major groove to the 5′-face of the modified adenine (*27*). These stereochemically induced structural differences are discussed in relation to the results of site-directed mutagenesis studies with these adducts, which revealed the SRSR(61,2) adduct was less mutagenic than the RSRS(61,2) adduct (*43*).

MATERIALS AND METHODS

Materials. The oligodeoxynucleotide 5′-d(CTTCTTGTCCG)-3′ was purchased from Midland Certified Reagent Co. (Midland, TX). The modified oligodeoxynucleotide 5′-d(CGGAC^{S,R,S,R}AAGAAG)-3′ (Chart 1) was synthesized through a procedure in which (±)-aminotriol derived from (±)-4*β*,3α-dihydroxy-2α,1α-epoxy-1,2,3,4-tetrahydrobenz[*a*]anthracene [(±)-DE2] was reacted with an oligodeoxynucleotide containing 6-fluoroadenosine at position X^6 (*30*−*32*). The (1*S*,2*R*,3*S*,4*R*)-N^6-[1-(1,2,3,4-tetrahydro-2,3,4-trihydroxybenz[*a*]anthracenyl)]-2′-deoxyadenosyl-modified oligodeoxynucleotide was purified from the reaction mixture by HPLC using a reverse-phase semipreparative column (PRP-1; Hamilton Co., Reno, NV) equilibrated with 10 mM ethylenediamineacetate (pH 7.0). The oligodeoxynucleotide

was eluted with a gradient from 0 to 20% acetonitrile in 20 min. It was identified using multiple methods, including circular dichroism spectroscopy, enzymatic digestion, and mass spectroscopy. The DNA was lyophilized and desalted on Sephadex G-25 (Amersham-Pharmacia, Inc., Piscataway, NJ).

NMR Samples. The oligodeoxynucleotide concentrations were determined from extinction coefficients of 1.09×10^5 M^{-1} cm^{-1} for modified and 9.24×10^4 M^{-1} cm^{-1} for the complementary strands, at 260 nm (*47*). The complementary oligodeoxynucleotides were mixed at a 1:1 molar ratio in 0.1 M NaCl, 10 mM NaH_2PO_4, and 50 μM Na_2EDTA (pH 7). The mixture was heated to 90 °C for 5 min and was cooled to room temperature. DNA grade Bio-Gel hydroxylapatite (Bio-Rad Laboratories, Hercules, CA) (15 cm × 3.0 cm), eluted with a gradient from 10 to 200 mM NaH_2PO_4 (pH 7.0), was used for the separation of double- and single-stranded oligodeoxynucleotides. The duplex was lyophilized and dissolved in 0.5 mL of H_2O, and desalted on Sephadex G-25 (70 cm × 1.5 cm). The sample was lyophilized and redissolved in 0.25 mL of NMR buffer containing 0.1 M NaCl, 10 mM NaH_2PO_4, and 50 μM Na_2EDTA (pH 7.0). The solution was lyophilized and exchanged three times with 99.96% D_2O. The strand concentrations of the samples were approximately 1.7 mM. The samples used for examining nonexchangeable protons were dissolved in 99.996% D_2O buffer. The samples used for the examination of the exchangeable protons were in buffer solution containing 9:1 H_2O/D_2O.

UV Melting. The experiments were carried out on a Cary 4E spectrophotometer (Varian Associates, Palo Alto, CA). The buffer was 10 mM sodium phosphate, 0.05 mM Na_2-EDTA, and 1 M NaCl (pH 7.0). The buffer solution was degassed prior to the experiment. The concentrations were adjusted to 4.8×10^{-6} M in a 1 cm cuvette. The temperature was increased at a rate of 0.5 °C/min from 2 to 90 °C. Absorbance was measured at 260 nm. The melting temperatures of the native and modified oligodeoxynucleotides were calculated by determining the midpoints of the melting curves from the first-order derivatives.

NMR. Experiments were performed at ^1H frequencies of 750.13, 600.13, and 500.13 MHz. To examine exchangeable protons, phase-sensitive NOESY experiments were carried out in 9:1 H_2O/D_2O buffer at a ^1H frequency of 600.13 MHz. The Watergate pulse sequence suppressed the water signal (*48*). The spectra were recorded at 5 °C with a mixing time of 250 ms. The phase-sensitive NOESY spectra used in the nonexchangeable proton resonance assignments were recorded at 10 °C using TPPI quadrature detection with a mixing time of 250 ms. To derive the distance restraints from NOESY experiments, three spectra were recorded consecutively with mixing times of 100, 150, and 250 ms. In these experiments, the data were recorded with 512 real data points in the t_1 dimension and 4096 real data points in the t_2 dimension. The relaxation delay was 2 s. The data were processed using FELIX (version 97.0, Molecular Simulations, Inc., San Diego, CA) on Silicon Graphics (Mountain View, CA) Octane workstations. The data in the t_1 dimension were zero-filled to give a matrix of 2K × 2K real points. A skewed sine-bell-square apodization function with a 90° phase shift was used in both dimensions.

Generation of Restraints. Footprints were drawn around the NOE cross-peaks for the NOESY spectrum measured with a mixing time of 250 ms to define the size and shape of the individual cross-peaks using FELIX. The same set of footprints was applied to spectra measured with other mixing times. Cross-peak intensities were determined by volume integration of the areas under the footprints. The intensities were combined as necessary with intensities generated fromcomplete relaxation matrix analysis of a starting DNA structure to generate a hybrid intensity matrix (*49*). MARDIGRAS (version 3.0) (*50*, *51*) refined the hybrid matrix by iteration to optimize the agreement with experimental NOE intensities. The molecular motion was assumed to be isotropic. Calculations, generally requiring two to five cycles, were performed using DNA starting models generated by INSIGHTII (version 97.0), the three mixing time NOE experiments, with six τ_c values (2, 3, 4, 5, 6, and 7 ns). The resulting sets of distances were averaged to give the experimental NOE restraints used in subsequent molecular dynamics calculations (*45*). For partially overlapped cross-peaks, lower or upper error bounds on the resulting distances were increased. The distance restraints were divided into five classes on the basis of the confidence factor obtained from MARDIGRAS.

Additional restraints were included for base pairs distal to the adduct site (i.e., other than the modified base pair and its nearest neighbors). The inclusion of these restraints was based upon spectroscopic data showing that the distal base pairs were unchanged from the B-like geometry of the unmodified *ras61* duplex (*22*); i.e., the perturbations introduced by the benz[*a*]anthracene were localized. The deoxyribose data for distal base pairs were consistent with the C2′-endo sugar ring conformation (*52*). Except for the modified nucleotide and immediately adjacent base pairs, the deoxyribose rings were restrained to the C2′-endo conformation. Except for the adduct site and immediately adjacent base pairs, the backbone torsion angles ϵ and ζ were restrained to 165 ± 35° and 245 ± 35°, respectively (*53*). Empirical Watson−Crick hydrogen bonding restraints between base pairs were used except for the adducted $^{S,R,S,R}A^6$•T^{17} base pair. These were consistent with crystallographic data (*54*) and similar to those used previously in structural determinations of oligodeoxynucleotides (*55*, *56*).

Restrained Molecular Dynamics. Calculations were performed using X-PLOR (version 3.85) (*57*). The force field was derived from CHARMM (*58*) and adapted for restrained MD calculations of nucleic acids. The empirical energy function (*58*) consisted of terms that could be individually manipulated for bonds, bond angles, torsion angles, tetrahedral and planar geometry, hydrogen bonding, and nonbonded interactions, including van der Waals and electrostatic forces. It treated hydrogens explicitly. The van der Waals energy term used the Lennard-Jones potential energy function. The electrostatic term used the Coulomb function, based on a full set of partial charges (−1/residue) and a distance-dependent dielectric constant of 4. The nonbonded pair list was updated if any atom moved more than 0.5 Å, and the cutoff radius for nonbonded interactions was 11 Å. Calculations were performed in vacuo without explicit counterions. Final structures were analyzed using X-PLOR to determine the rmsd between an average structure and the converged structures. Back-calculation of theoretical NMR intensities

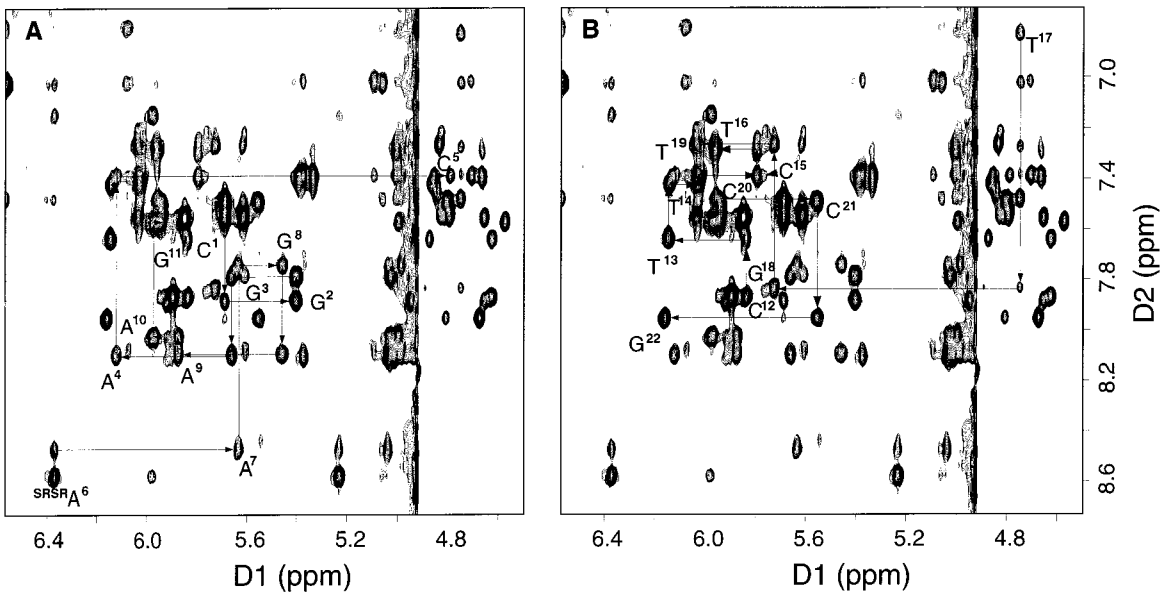

FIGURE 1: Expanded plots from the aromatic−anomeric region of the 750.13 MHz NOESY spectrum at 10 °C using a 250 ms mixing time. Sequential NOE connectivities for (A) the modified strand and (B) the complementary strand.

from the emergent structures was performed using CORMA (version 4.0) (*49*). The structures were analyzed using DIALS AND WINDOWS 1.0 (*59*).

Method 1. Thirty starting structures with random coordinates were generated using X-PLOR. These were subjected to a simulated annealing protocol substantially similar to that described in the X-PLOR manual for initial folding (*57*, *60*). The resulting structures were then submitted to a simulated annealing procotol to reach a "global fold" (*46*, *61*, *62*). During the initial and global fold stage, all electrostatic interactions were turned off. The repulsive van der Waals potential was used. Experimental NOE and hydrogen bond distance restraints were used. Subsequently, the "globally folded" intermediate structures were subjected to a refinement stage of restrained molecular dynamics utilizing a simulated annealing protocol that included NOE, torsion angle restraints, and empirical restraints. Calculations were initiated by coupling to a heating bath with a target temperature of 900 K, with force constants of 10 kcal mol^{-1} Å^{-2} for empirical hydrogen bonding, 20 kcal mol^{-1} Å^{-2} for torsion angle restraints, and 50, 45, 40, 35, and 30 kcal mol^{-1} Å^{-2} for the five classes of NOE restraints. The target temperature was reached in 5 ps and was maintained for 6 ps. The molecules were cooled to 300 K over the course of 5 ps and maintained at that temperature for 15 ps of equilibrium dynamics. The force constants for the five classes of NOE restraints were scaled up for 3−5 ps during the heating period to 150, 130, 100, 100, and 100 kcal mol^{-1} Å^{-2} in the order of confidence factor. These weights were maintained during the reminder of the heating period and for the first 2 ps of the equilibrium dynamics period. They were then scaled down to 50, 45, 40, 35, and 30 kcal mol^{-1} Å^{-2} in the order of confidence factor. The torsion angle and base pair distance force constants were scaled up to 100 kcal mol^{-1} Å^{-2} during the same period that was used for the NOE restraints. They were scaled back to 20 kcal mol^{-1} Å^{-2}, also at the same time as the NOE restraints. Coordinate sets were archived every 0.1 ps, and 49 structures from the last 5 ps were averaged. These average rMD structures were subjected to 1100 iterations of conjugate gradient energy minimization so the final structures could be obtained.

Method 2. Two starting structures were built from B-DNA and A-DNA using INSIGHTII (version 97.0) such that the BA moiety intercalated between ^{S,R,S,R}A^{6}•T^{17} and A^{7}•T^{16}. Restrained molecular dynamics calculations utilized the simulated annealing protocol as described above for the refinement stage in Method 1.

RESULTS

Thermal Stability. The thermal stability of the BA SRSR-(61,2) adduct was examined by UV melting studies which compared it with the unadducted *ras61* sequence. The measured T_m was 45 °C. The SRSR(61,2) adduct destabilized the duplex, as indicated by a 9 °C reduction in the T_m compared to that of the unmodified duplex, which melted at 54 °C. A series of one-dimensional ^{1}H spectra obtained at temperatures ranging from 10 to 35 °C indicated that 10 °C is the optimal temperature at which the duplex remained intact, and the ^{1}H resonances were the sharpest and best resolved.

^{1}H Resonance Assignments. (a) Nonexchangeable Protons. The BA lesion interrupted the sequential NOE connectivities of B-form DNA at C^5, the 5′-neighbor of the adducted adenine in the modified strand (Figure 1). No NOE connectivity was observed between C^5 H1′ or H2″ and ^{S,R,S,R}A^6 H8. The intranucleotide NOE between C^5 H1′ and C^5 H6 was weaker than that observed in B-DNA. NOE connectivities for the reminder of the modified strand had intensities as expected for B-DNA. In the complementary strand, interruption of the sequential NOEs was observed between T^{16} H1′ or H2″ and T^{17} H6. The internucleotide connectivity between T^{17} H1′ and G^{18} H8 was weaker than the corresponding NOEs observed for nucleotides far from the site of the lesion. The assignments of the remaining deoxyribose protons were determined from a DQF-COSY spectrum. The H5′ and H5″ resonances were subject to substantial overlap but were partially assigned. In instances where these resonances were observed, the stereospecific assignments of

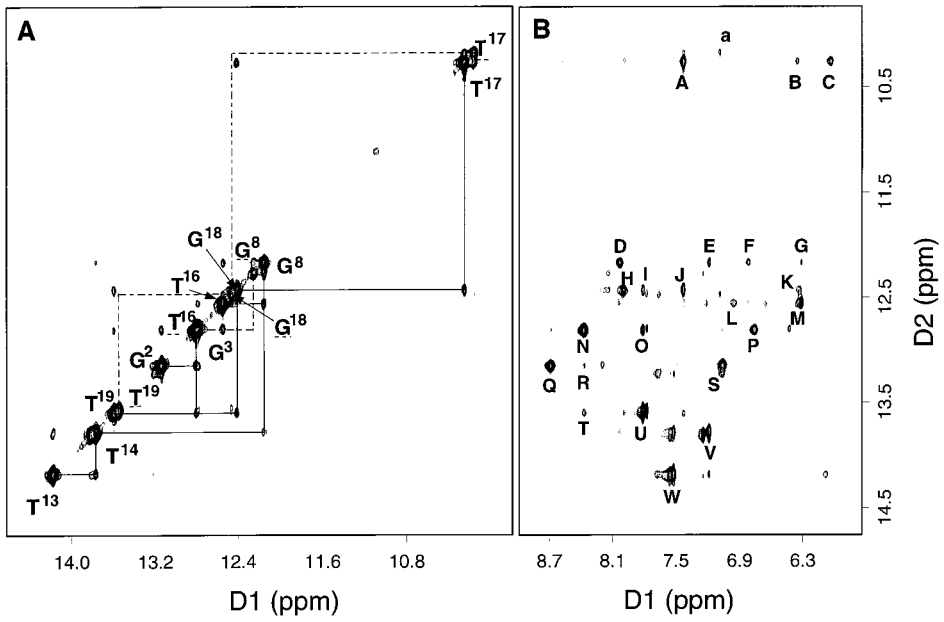

FIGURE 2: (A) Expanded plot showing sequential NOE connectivities for the imino protons. The connectivities are traced with solid lines for the major conformation and with dashed lines for the minor conformation. The labels represent the imino protons of the designated bases. (B) Expanded plot showing NOE connectivities between imino protons and the amino, base, and benz[*a*]anthracene protons: cross-peaks A−C, T^{17} N3H → $^{S,R,S,R}A^6$ H2, BA H12, and $^{S,R,S,R}A^6$ N6H_a, respectively; cross-peaks D−G, G^8 N1H → C^{15} N4H_a, A^9 H2, C^{15} N4H_b, and A^7 H2, respectively; cross-peaks H−K, G^{18} N1H → C^5 N4H_a, A^4 H2, $^{S,R,S,R}A^6$ H2, and C^5 N4H_b, respectively; cross-peaks L and M, T^{16} N3H → BA H10 and A^7 H2, respectively; cross-peaks N−P, G^3 N1H → C^{20} N4H_a, A^4 H2, and C^{20} N4H_b, respectively; cross-peaks Q−S, G^2 N1H → C^{21} N4H_a, C^{20} N4H_a, and C^{21} N4H_b, respectively; cross-peaks T and U, T^{19} N3H → C^{20} N4H_a and A^4 H2, respectively; cross-peak V, T^{14} N3H → A^9 H2; cross-peak W, T^{13} N3H → A^{10} H2; and cross-peak a, T^{17} N3H → $^{S,R,S,R}A^6$ H8 in the minor conformation. The 600.13 MHz NOESY spectrum was collected with a mixing time of 250 ms and at 5 °C.

H5′ and H5″ were made empirically. There were no cross-peaks between purine H8 or pyrimidine H6 resonances to any deoxyribose H5′ and H5″ resonances that were as large as the H6/H8−H1′ cross-peaks. All H2′−H5′/H5″ cross-peaks were weaker than H2′−H1′ cross-peaks. This suggested that the backbone torsion angle γ was in all instances within the range of 60 ± 40°. Accordingly, the expected distance between H3′ and H5″ was smaller than the expected distance between H3′ and H5′. Due to spin diffusion, it was generally not possible to directly evaluate relative cross-peak intensities directly from the spectrum. Instead, the assignments of H5 and H5″ were empirically adjusted following MARDIGRAS calculations to satisfy the anticipated distance bounds for torsion angle γ. In general, H5″ resonated downfield of H5′. The chemical shifts of the nonexchangeable protons are listed in Table S1 in the Supporting Information.

(b) Exchangeable Protons. Assignments of the imino protons were made from NOE cross-peaks between adjacent base pairs and connectivities to the base-paired amino protons (*63*). An expanded region showing cross-peaks between the imino protons in both conformations is given in Figure 2A. An interruption of the sequential imino-to-imino proton NOEs of adjacent base pairs was found between T^{17} N3H and T^{16} N3H in both conformations. There were large upfield shifts for T^{16} N3H and T^{17} N3H (12.5 and 10.3 ppm), in comparison to the corresponding resonances of the unadducted duplex (*22*). The strong cross-peak between $^{S,R,S,R}A^6$ H2 and T^{17} N3H indicated the presence of hydrogen bonding between $^{S,R,S,R}A^6$ and T^{17}. The chemical shifts of the exchangeable protons are listed in Table S2 of the Supporting Information.

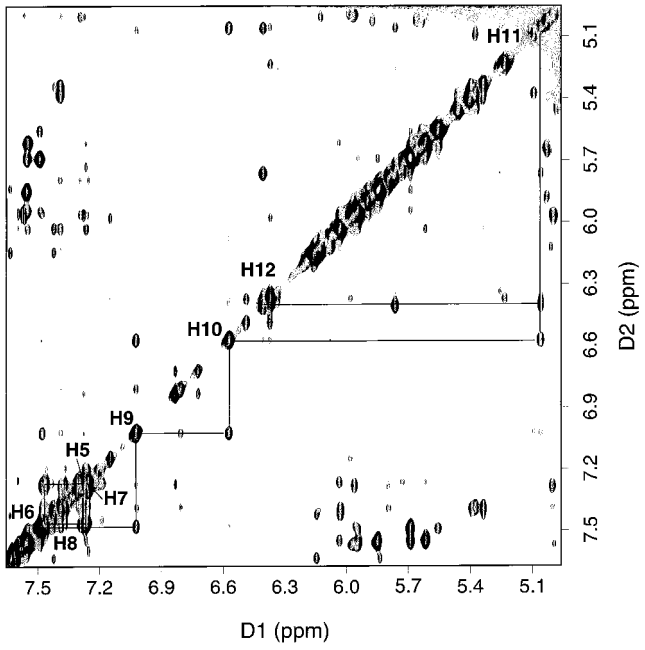

FIGURE 3: Expanded 750.13 MHz NOESY spectrum with a mixing time of 250 ms showing the assignments for the aromatic protons of BA. The experiment was carried out at 10 °C.

(c) Benz[a]anthracene Protons. The anthracenyl protons were assigned by the combined use of DQF-COSY and NOESY spectra (Figure 3). The numbering scheme for the BA protons is shown in Chart 1. A strong NOE was found between H12 and a resonance at 5.77 ppm. This was assigned to H1. A strong cross-peak was detected between H1 and a resonance at 4.41 ppm. This was assigned to H2. A weak cross-peak was detected between H1 and a resonance at 3.75 ppm. This was assigned to H3. The other aliphatic ring proton

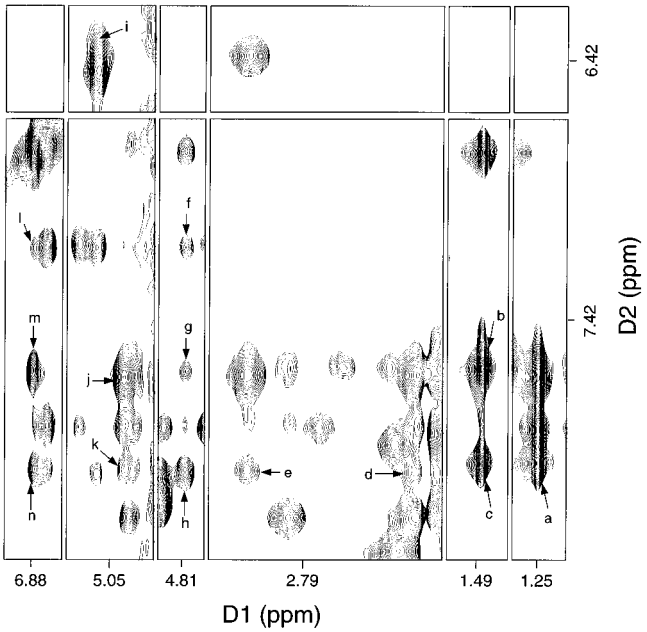

FIGURE 4: Tile plot showing NOE cross-peaks between nonexchangeable protons of DNA and BA protons: cross-peak a, T^{16} CH_3 → BA H6; cross-peaks b and c, T^{17} CH_3 → BA H5 and H6, respectively; cross-peaks d and e, T^{16} H2′ and H2″ → BA H8, respectively; cross-peaks f−h, T^{17} H1′ → BA H9, H7, and H8, respectively; cross-peak i, $^{S,R,S,R}A^6$ H1′ → BA H11; cross-peaks j and k, T^{16} H3′ → BA H6 and H7, respectively; and cross-peaks l−n, T^{17} H6 → BA H9, H7, and H8, respectively.

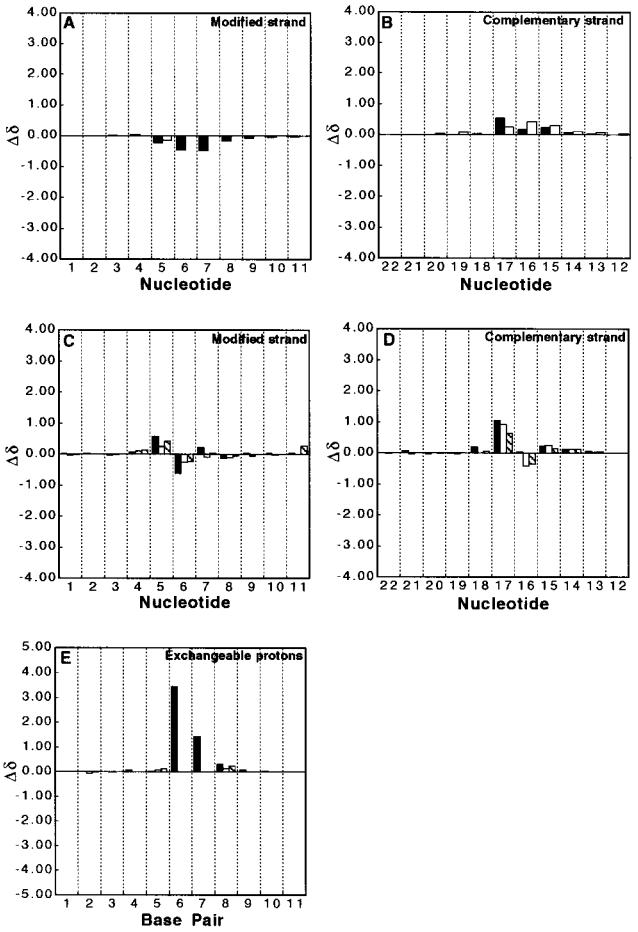

FIGURE 5: Chemical shift changes of selected protons relative to the unmodified oligodeoxynucleotide duplex. (A and B) Major groove protons in the modified and complementary strands, respectively: black bars, G/A H8 or C/T H6; and white bars, C H5 or T CH_3. (C and D) Minor groove protons in the modified and complementary strands, respectively: black bars, H1′; white bars, H2′; and crosshatched bars, H2″. (E) Exchangeable protons: black bars, G N1H or T N3H; white bars, C N4H(a); and crosshatched bars, C N4H(b). $\Delta\delta = \delta_{\text{unmodified-oligodeoxynucleotide}} - \delta_{\text{modified-oligodeoxynucleotide}}$ (parts per million).

H4 had no distinct resonances with either BA or DNA protons, and therefore was not assigned. The chemical shifts of the benz[*a*]anthracenyl resonances are listed in Table S3 of the Supporting Information.

Benz[a]anthracene−DNA NOEs. There were 40 NOEs between the BA and DNA protons. Some of these are shown in Figure 4. The benz[*a*]anthracene aromatic protons H5−H7, located on the same face of the benz[*a*]anthracene moiety, exhibited cross-peaks to T^{16} and T^{17} CH_3 and H6. Benz[*a*]anthracene H7−H9 exhibited cross-peaks to T^{16} and T^{17} H1′. Benz[*a*]anthracene H6 and H7 exhibited cross-peaks to T^{16} H3′. Cross-peaks were observed between H11 and H12, located on the opposite face of the benz[*a*]anthracene moiety from H5 to H7, and A^6 H1′. Cross-peaks were also observed between H10 and H12 of benz[*a*]anthracene and the exchangeable protons T^{16} N3H and T^{17} N3H (Figure 2B).

Chemical Shift Perturbations. The chemical shifts of the nonexchangeable and exchangeable protons, compared to those of the unmodified *ras61* sequence, are shown in Figure 5. The greatest upfield shift (3.44 ppm) was observed for T^{17} N3H, the imino proton of the adducted base pair. The imino proton of A^7·T^{16} also experienced an upfield shift of 1.43 ppm. Downfield chemical shifts of 0.65 and 0.63 ppm were observed for T^{16} H2′ and H2″, respectively. A^6 H8 and A^7 H8 shifted downfield 0.87 ppm. A^6 H1′ also shifted downfield 0.62 ppm. Upfield chemical shift changes of 0.58 and 1.05 ppm were observed for C^5 and T^{17} H1′, respectively. Upfield chemical shift changes of 0.92 and 0.64 ppm were also observed for T^{17} H2′ and H2″, respectively. Other smaller upfield shifts were observed for a number of protons near the adduction site.

Experimental Restraints. There were 477 experimental distance restraints derived from nonexchangeable ^{1}H NOEs by MARDIGRAS. These consisted of 306 intranucleotide restraints, 133 internucleotide restraints, and 38 BA−DNA restraints. The distribution of these restraints for each base is summarized in Figure 6. The restraints were approximately evenly distributed along the length of the oligodeoxynucleotide. The smaller numbers of restraints for some nucleotides, e.g., A^7, were generally due to overlapping resonances, preventing accurate measurement of cross-peak intensities. Another exception was C^5, which exhibited no internucleotide restraints with A^6. A list of experimental distance restraints along with the upper and lower bounds is shown in Table S4 of the Supporting Information.

Structural Refinement. Two approaches were used. The first approach utilized methodology described by Tinoco and co-workers (*61*, *62*), and further developed by Allain and Varani (*46*, *64*). Calculations were begun from random coordinates as generated by X-PLOR. In the first stage of refinement, NOE and hydrogen bonding distance restraints (except at the adducted base pair) only were utilized to determine the "global fold" of the oligodeoxynucleotide. Beginning with 30 independently calculated structures having random coordinates, seven "converged" structures were

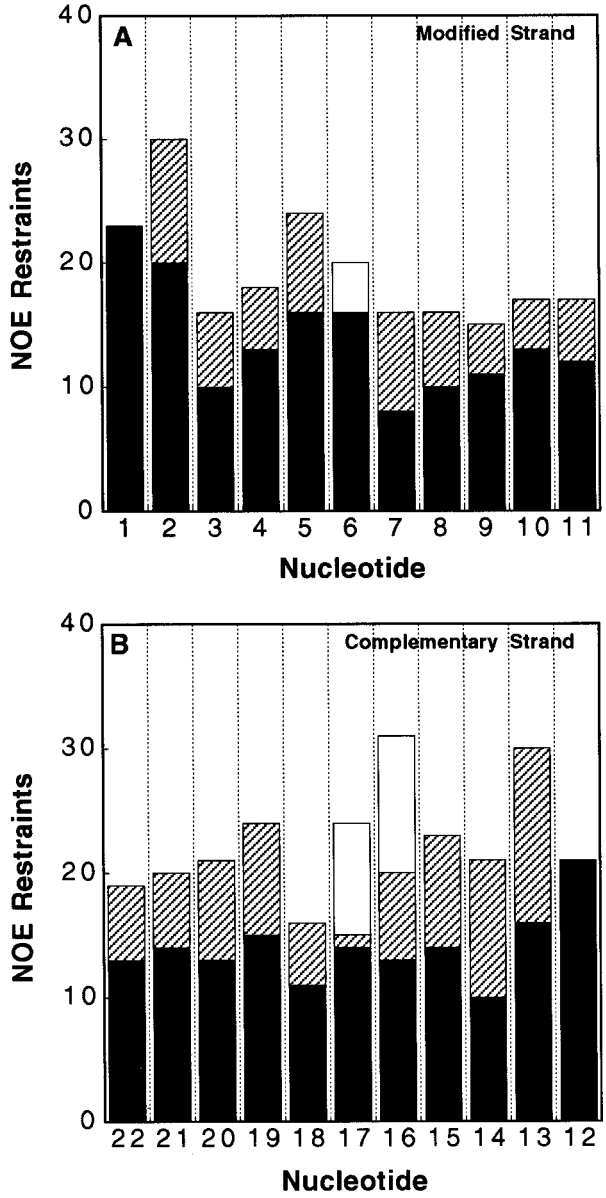

FIGURE 6: Distribution of experimental NOE restraints applied in the structural refinement for the (A) modified strand and (B) complementary strand: crosshatched bars, internucleotide NOEs; black bars, intranucleotide NOEs; and white bars, BA−DNA NOEs. The internucleotide NOEs are counted in the direction from *n* to *n* − 1.

obtained. Convergence was evaluated using energy, energy-ordered rmsd profiles (*64*, *65*), and the R_x factor. The total energies and NOE restraint violation energies for converged structures were lower than 3 and 0.1 kcal/mol, respectively. The maximum pairwise rmsd for the converged structures was 0.8 Å, indicating a well-defined conformation. Theoretical NOE intensities calculated from complete relaxation matrix analysis for the refined structures, and compared to the experimental intensities, yielded sixth-root residuals (*49*) of approximately 10%, both for intranucleotide NOEs and for internucleotide NOEs (Table 1). Figure 7 depicts in detail the R_1^x values as a function of nucleotide, in the adducted duplex, neglecting the terminal base pairs.

The second approach utilized methodology developed by James and co-workers (*45*). This method had successfully generated solution structures for other PAH adducts in the *ras61* oligodeoxynucleotide (*26*, *27*, *66*). The principal difference between the two approaches was in the choice of starting structures for the molecular dynamics calculations. The second approach used starting structures based upon canonical A-form and B-form DNA duplexes, in which the benz[*a*]anthracene adduct was intercalated. The refined structures obtained from either approach were similar, as judged by a rmsd of 1.5 Å. The structural data reported in Table 1 were derived from the calculations initiated from random coordinates.

Table 1: Analysis of the MD-Generated Structures of the BA SRSR(61,2) Adduct

NMR restraints	
total no. of distance restraints	477
no. of inter-residue distance restraints	133
no. of intra-residue distance restraints	306
no. of DNA−BA distance restraints	38
empirical restraints	
no. of H-bonding restraints	26
no. of dihedral planarity restraints	18
no. of sugar pucker restraints	80
no. of backbone torsion angle restraints	32
structural statistics	
NMR *R*-factor (R_1^x)[a−c]	
⟨rMDRi⟩	0.0974 ± 0.0009
rmsd of NOE violations (Å)	0.064 ± 0.002
no. of NOE violations >0.2 Å in the entire duplex	13 ± 2
root-mean-square deviations from ideal geometry	
bond lengths (Å)	0.0246 ± 0.0003
bond angles (deg)	1.943 ± 0.008
improper angles (deg)	0.44 ± 0.03
pairwise rmsd (Å) over all atoms	
⟨rMDRi⟩ vs ⟨rMDav⟩	0.77 ± 0.04

[a] Only the inner nine base pairs were used in the calculations, to exclude end effects. The mixing time was 250 ms. All values for R_1^x are $\times 10^2$. [b] $R_1^x = \Sigma|(a_o)_i^{1/6} - (a_c)_i^{1/6}|/\Sigma|(a_o)_i^{1/6}|$, where a_o and a_c are the intensities of observed (non-zero) and calculated NOE cross-peaks, respectively. [c] ⟨rMDRi⟩ , seven converged structures starting from random coordinates; ⟨rMDav⟩, average of seven converged structures.

Figure 8 shows a stereoview of seven converged structures derived from rMD calculations starting with random coordinates. The stick-ribbon model shown in Figure 9 represents one final structure. The refined structure was a right-handed duplex, in which the BA moiety intercalated from the major groove between ^{S,R,S,R}A^6•T^{17} and A^7•T^{16}. The saturated ring of BA was oriented in the major groove of the duplex, with the aromatic rings inserted into the duplex such that the terminal ring of BA threaded the duplex and faced toward the minor groove direction. The duplex suffered localized distortion at and immediately adjacent to the adduct site, evidenced by the increased rise of 8.7 Å compared to the value of 3.5 Å normally observed for B-DNA between base pairs ^{S,R,S,R}A^6•T^{17} and A^7•T^{16}. These two base pairs also buckled in opposite directions away from the intercalated BA moiety. Changes of 74° and −28° in buckle were calculated for ^{S,R,S,R}A^6•T^{17} and A^7•T^{16}, respectively. The calculated structures predicted that T^{17} was twisted out of plane, as indicated by a −29° change in propeller twist for ^{S,R,S,R}A^6•T^{17}. The BA adduct was accommodated in the DNA duplex without helical bending. The distortion in the duplex was localized, such that base pairs removed from the adduct site appeared to remain in a B-like conformation.

Conformational Exchange. The existence of two conformations was apparent in both one- and two-dimensional

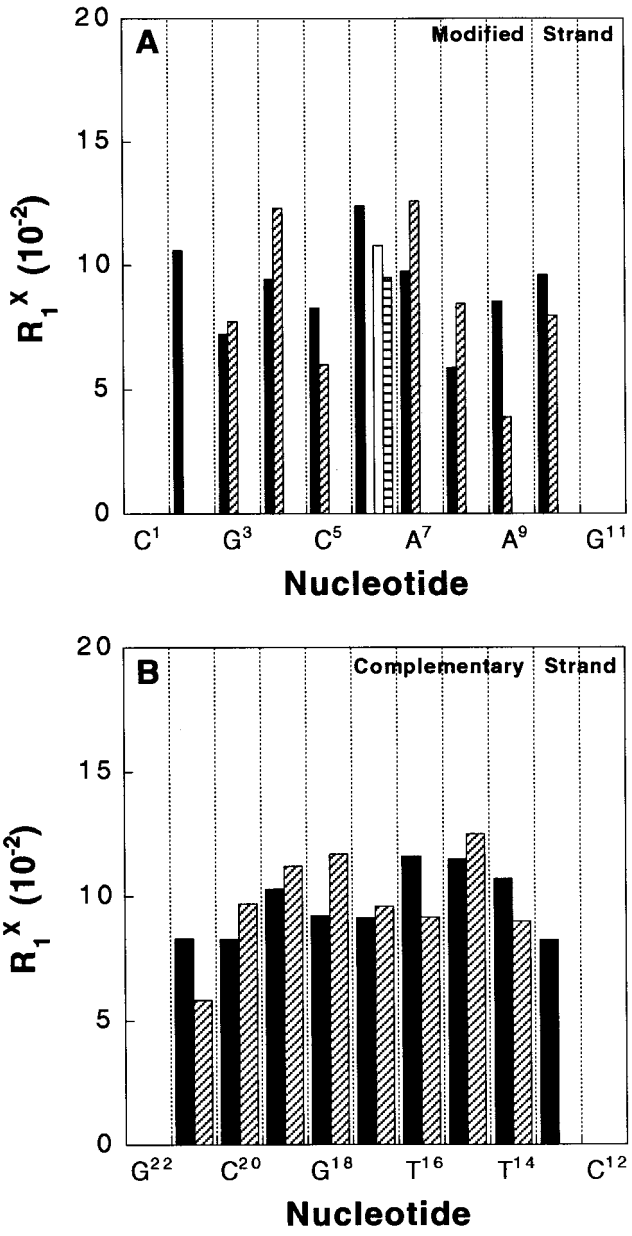

FIGURE 7: Bar diagrams showing the per-residue R_1^x values for the modified and complementary strands of the BA SRSR(61,2) adduct where the black bars show the intraresidue R_1^x values, the crosshatched bars show the inter-residue R_1^x values, the white bar shows the interstrand R_1^x values between $^{S,R,S,R}A^6$ and T^{16}, and the horizontally hatched bar shows the interstrand R_1^x values between $^{S,R,S,R}A^6$ and T^{17}.

NMR spectra. The observation of 15 identifiable resonances (Figure 10) in the imino proton region (10−15 ppm) of the one-dimensional spectrum contrasts with the nine imino proton resonances observed for the unmodified 11-mer duplex (*22*). Exchange cross-peaks were observed in NOESY spectra recorded at 10 and 25 °C (Figure 11A) and a ROESY spectrum (Figure 11B). The total contribution of minor conformer to the BA-modified duplex at 10 °C was estimatedto be 20%. This was determined by measuring cross-peak volumes for T^{17} H6−T^{17} CH_3 NOEs for each conformation from a NOESY spectrum recorded at 10 °C with a mixing time of 100 ms.

The nonexchangeable protons in the minor conformation were partially assigned. Compared to the major conformation, $^{S,R,S,R}A^6$ H8 shifted upfield from 8.64 to 7.20 ppm. C^5 H6

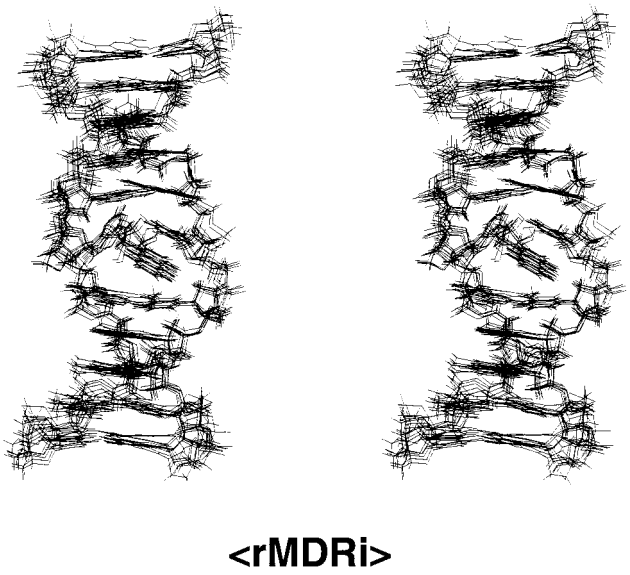

FIGURE 8: Stereoviews showing the comparisons of seven superimposed ⟨rMDRi⟩ structures.

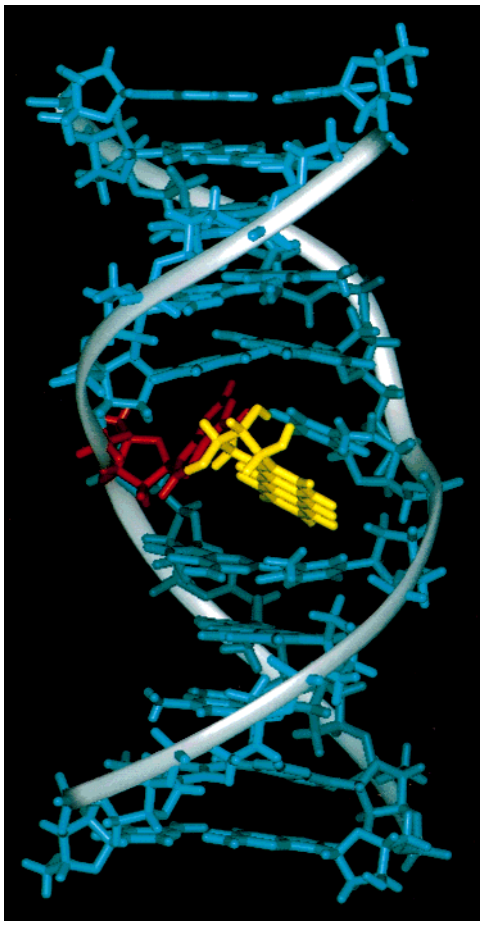

FIGURE 9: Stick-ribbon model representation of one final structure. The BA moiety is yellow.

shifted upfield from 7.45 to 7.08 ppm. A^6 H1′ shifted upfield from 6.42 to 6.04 ppm. A striking spectral feature of the minor conformer was the very strong NOE cross-peak between $^{S,R,S,R}A^6$ H8 and its sugar H1′, whose intensity (100 ms mixing time) was as large as that of the BA H9−H10 cross-peak. This strong intraresidue NOE between H8 and H1′ indicated a syn glycosidic torsion angle (*67*) at the

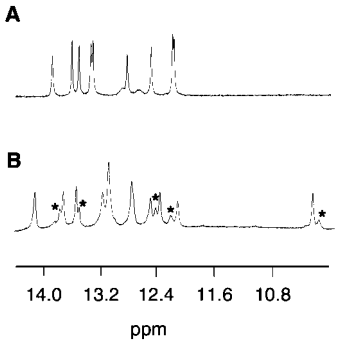

FIGURE 10: One-dimensional 500.13 MHz ^{1}H NMR spectra of the imino proton region: (A) the unmodified *ras61* duplex and (B) the modified duplex at 5 °C.

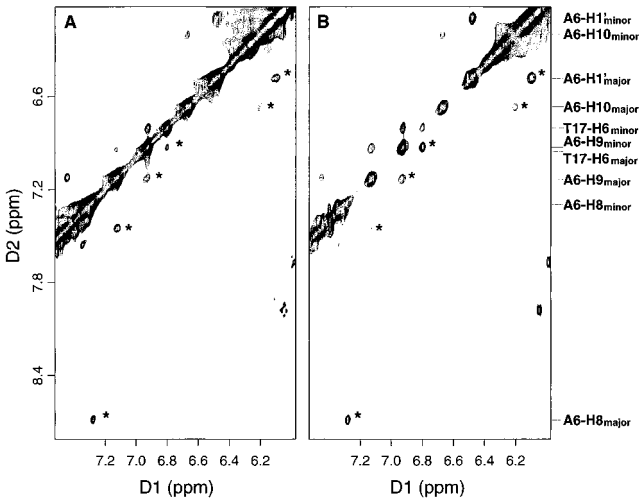

FIGURE 11: (A) Expanded region of the 500.13 MHz NOESY spectrum with a mixing time of 20 ms. (B) Expanded region of the 500.13 MHz ROESY spectrum with a mixing time of 150 ms. Both experiments were carried out at 25 °C. Exchange cross-peaks are labeled with an asterisk (*).

modified $^{S,R,S,R}A^6$. There were large upfield shifts for T^{16} N3H and T^{17} N3H in both conformations (12.54 and 10.27 ppm for the major conformation, and 12.81 and 10.17 ppm for the minor conformation), in comparison to those of the corresponding resonances of the unadducted duplex (*22*). In the minor conformation, $^{S,R,S,R}A^6$ H8, observed at 7.20 ppm, exhibited a NOE to the imino proton of $^{S,R,S,R}A^6$•T^{17}, observed at 10.17 ppm (Figure 2B).

DISCUSSION

This research program seeks to examine structure−activity relationships for a series of site-specific adenyl N^6 PAH adducts, in an effort to relate the chemical structures and solution conformations of these adducts with their corresponding mutagenic potentials. The work presented here defines the structural perturbations induced at position (61,2) of the *ras61* oligomer by the BA SRSR(61,2) adduct, a site at which mutations activate the *N-ras* protooncogene. The results reveal that the major conformation of the BA SRSR(61,2) adduct is one in which the PAH moiety is intercalated 3′ to the lesion site. A minor conformation is also present, in which the modified $^{S,R,S,R}A^6$ nucleotide is rotated into the syn conformation about the glycosidic bond. In the following discussion, our intent is to examine the structure of the SRSR(61,2) adduct in detail, to compare its structure with other PAH adducts at adenine N^6 having the (*S*)-configuration about the benzylic carbon, and to examine the implications of these structural revelations upon mutagenesis.

Solution Conformation of the BA SRSR(61,2) Adduct. The adducted BA moiety intercalated into the DNA duplex from the major groove, and in the 3′-direction from the modified nucleotide $^{S,R,S,R}A^6$. To accommodate this, the rMD calculations predicted increased buckling for base pairs $^{S,R,S,R}A^6$•T^{17} and A^7•T^{16}, relative to that of the unmodified *ras61* oligodeoxynucleotide. The increased rise of 8.7 Å as compared to the value of 3.5 Å normally observed for B-DNA between base pairs $^{S,R,S,R}A^6$•T^{17} and A^7•T^{16} was consistent with intercalation. The calculated structures predicted that both A^7 and T^{17} were buckled out of plane, as indicated by 74° and −28° changes in buckle for $^{S,R,S,R}A^6$•T^{17} and A^7•T^{16}, respectively. This was attributed to alleviation of steric clash with the BA hydroxyl groups. The out-of-plane twisting positioned T^{17} such that the intercalated BA moiety stacked with the A^7 in the modified strand and with T^{17} in the complementary strand.

The rMD calculations predicted Watson−Crick base pairing was weakened at base pair $^{S,R,S,R}A^6$•T^{17}, a consequence of weakened hydrogen bonding. This was consistent with the 10 ± 1 °C reduction in the T_m of the $^{S,R,S,R}A^6$-modified DNA duplex, which occurred despite the intercalation of the BA moiety into the helix and the stacking with A^7 and T^{17}. Stacking interactions between the BA moiety and A^7 and T^{17} were probably offset by poorer stacking involving the modified base $^{S,R,S,R}A^6$ and by weakening of hydrogen bonding at $^{S,R,S,R}A^6$•T^{17}.

The intercalation of the BA moiety in the 3′-direction was consistent with the pattern of NOEs from the BA moiety to base pair A^7•T^{16}. The orientation of the BA ring resulted in localization of the NOEs between the adduct and the DNA on the two faces of the anthracenyl ring. The BA aromatic protons H5−H7 exhibited NOEs to T^{16} and T^{17} CH_3 and H6, located in the major groove face of the DNA. The intercalation of the anthracenyl moiety oriented H7−H9 toward the deoxyribose moieties of T^{16} and T^{17} in the complementary strand; these protons exhibited NOEs to T^{16} and T^{17} H1′. NOEs between BA H11 and H12 and between $^{S,R,S,R}A^6$ H1′ were explained by the location of the bay ring beneath $^{S,R,S,R}A^6$. The imino protons T^{16} and T^{17} N3H were below and above the anthracenyl ring and exhibited an NOE to the BA aromatic protons H10 and H12. The expected NOE connectivity between the neighboring imino protons in base pairs A^7•T^{16} and $^{S,R,S,R}A^6$•T^{17} was missing, which in combination with the observed pattern of DNA−BA NOEs confirmed intercalation between these two base pairs.

The 2.4 ppm dispersion of the BA aromatic proton chemical shifts was consistent with intercalation of the PAH. This suggested that these protons existed in significantly different electronic environments. The rMD structures predicted that this is the case. Protons H5−H7 faced toward the major groove in a position less influenced by the ring currents of the adjacent nucleotide bases. The remaining BA protons were positioned such that ring current shielding from $^{S,R,S,R}A^6$, T^{16}, and T^{17} was anticipated. The orientation of the anthracenyl moiety explained the upfield chemical shifts of 1.1, 0.9, and 0.6 ppm, observed for T^{17} H1′, H2′, and H2″, respectively. These protons lay above the PAH ring. The 0.6 ppm upfield shift for C^5 H1′ and an unusual upfield shift

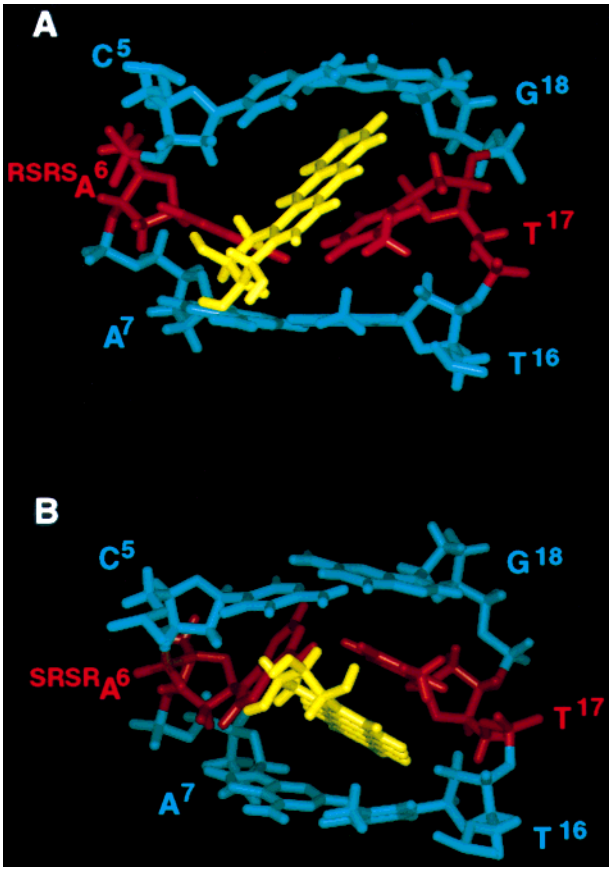

FIGURE 12: (A) Side view of the d($C_5A_6A_7$)-d($T_{16}T_{17}G_{18}$) segment of the BA RSRS(61,2) adduct from the major groove. **(B)** Side view of the d($C_5A_6A_7$)-d($T_{16}T_{17}G_{18}$) segment of the BA SRSR-(61,2) adduct from the major groove.

for BA aromatic proton H11 were explained by their orientations above and below the $^{S,R,S,R}A^6$ purine ring. The upfield shifts of the imino protons of base pairs A^7·T^{16} and $^{S,R,S,R}A^6$·T^{17} were also consistent with the intercalation model. Upfield shifts of 3.4 ppm for T^{17} N3H and 1.4 ppm for T^{16} N3H were consistent with insertion of the aromatic moiety into the helix.

Stereochemistry Effects. It was of interest to compare the structure of the BA SRSR(61,2) adduct reported in this paper with the corresponding structure of the BA RSRS(61,2) adduct (*27*). Both stereoisomers exhibited similar reductions in thermal stability as compared to the unmodified *ras61* duplex. In each instance, the thermal transition midpoints (T_m) for the modified duplexes were reduced by ~10 °C. The similar reductions in T_m indicated that the relative thermal stabilities of the BA SRSR(61,2) and RSRS(61,2) adducts were comparable. Both adducts preserved a right-handed B-like structure, except in the immediate vicinity of the modified site. The relative conformations of the two adducts extend our understanding of the effect of stereochemistry at the benzylic carbon on the adenyl N^6 series of PAH adducts. In all cases examined to date (*26*, *66*, *68*, *69*), the PAH adenyl N^6 adducts with (*R*)-stereochemistry at the benzylic carbon are oriented in the 5′-direction. In contrast, the corresponding adducts with (*S*)-stereochemistry at the benzylic carbon are oriented in the 3′-direction (Figure 12). This appears to be a general rule for adenine N^6 PAH adducts.

Existence of and Structural Analysis of a Minor Conformer. The partial assignments of ^{1}H resonances for the minor conformation indicated that the modified $^{S,R,S,R}A^6$ assumed a syn glycosidic torsion angle. This conclusion was supported by several lines of evidence. First, there was a strong NOE between $^{S,R,S,R}A^6$ H8 and its own sugar H1′, which was comparable in intensity to the NOE between BA H9 and H10. Second, there was a NOE between the imino proton of T^{17} and the H8 (rather than H2) of $^{S,R,S,R}A^6$, which could be possible only when the $^{S,R,S,R}A^6$ existed in the syn conformation. Third, an unusual downfield shift for the $^{S,R,S,R}A^6$ H3′ resonance (observed at 5.29 ppm) was consistent with an in-plane ring current effect caused by the adenine ring in a syn dA. Fourth, at 298 K, the NOE peak between dA^7 H8 and its own sugar H1′ became weak. This was consistent with broadening caused by rotation of the adenine ring of $^{S,R,S,R}A^6$ between anti and syn glycosidic torsion angles. There was also an unusual upfield shift for the A^6 H8 resonance (7.02 ppm). We have been unable to determine the orientation of the BA moiety in the minor conformation, but suspect that it remains intercalated and on the 3′-side of the modified $^{S,R,S,R}A^6$. This assertion is based upon the observation that the chemical shifts of the BA ring protons in the major and minor conformations are similar, suggesting a common environment for the BA moiety in each conformation. It also draws support from the refined structure of a RSRS benzo[*a*]pyrenyl adenyl N^6 adduct incorrectly paired with guanine (*70*). In that instance, the modified adenine was in the syn conformation about χ and the BP moiety was intercalated 3′ to the adduct site. For the PAH moiety to remain intercalated 3′ to the adduct site following rotation of the modified adenine about χ, a simultaneous rotation of torsion angles α' and β' (on either side of the linkage at adenine N^6) must occur. Thus, it is not surprising that there should be a relatively high energetic barrier separating these two conformational orientations, consistent with the observation that the two species are in slow exchange on the NMR time scale.

A Steric Basis for the Stability of the Intercalated BA SRSR(61,2) Adduct. The BA SRSR(61,2) structure provides insight into why this (1*S*)-BA adduct, and the previously examined (−)-*trans*-*anti*-benzo[*c*]phenanthrene−dA (BPh) adduct opposite dT (*41*), formed stable structures when placed opposite dT, with the PAH intercalated on the 3′-side of the lesion, while the BP RSRS(61,2) adduct with similar stereochemistry at the benzylic carbon, when placed opposite dT, was disordered (*26*). The BA SRSR(61,2) adduct conformation was similar to the BPh adduct opposite dT (*41*). For both of these adducts, the modified A·T base pair propeller twisted and buckled slightly to permit the BPh or BA to intercalate between the modified A·T and its 3′-neighbor base pair.

Chart 2 compares the geometries of the fused aromatic rings of BPh, BA, and BP. The BPh (*41*) and BA moieties intercalate easily into the DNA duplex 3′ to the modified adenine. The same is not true of the BP moiety; we suggest that the differing geometry of the BP aromatic rings causes this PAH to clash with the complementary strand of the DNA duplex when intercalated 3′ to the lesion site. To date, it has not been possible to refine a solution structure of the (10*S*)-BP adduct opposite its correct partner, thymine. A structure was determined in which the (10*S*)-BP adduct was placed

Chart 2: Spatial Relationships between the Pyrenyl Rings of (A) the SRSR Adenyl N^6 Benzo[*c*]phenanthrene Adduct As Examined by Cosman et al. (*41*), (B) the SRSR Adenyl N^6 Benz[*a*]anthracene Adduct (this work), and (C) the RSRS Adenyl N^6 Benzo[*a*]pyrene Adduct (*26*)[a]

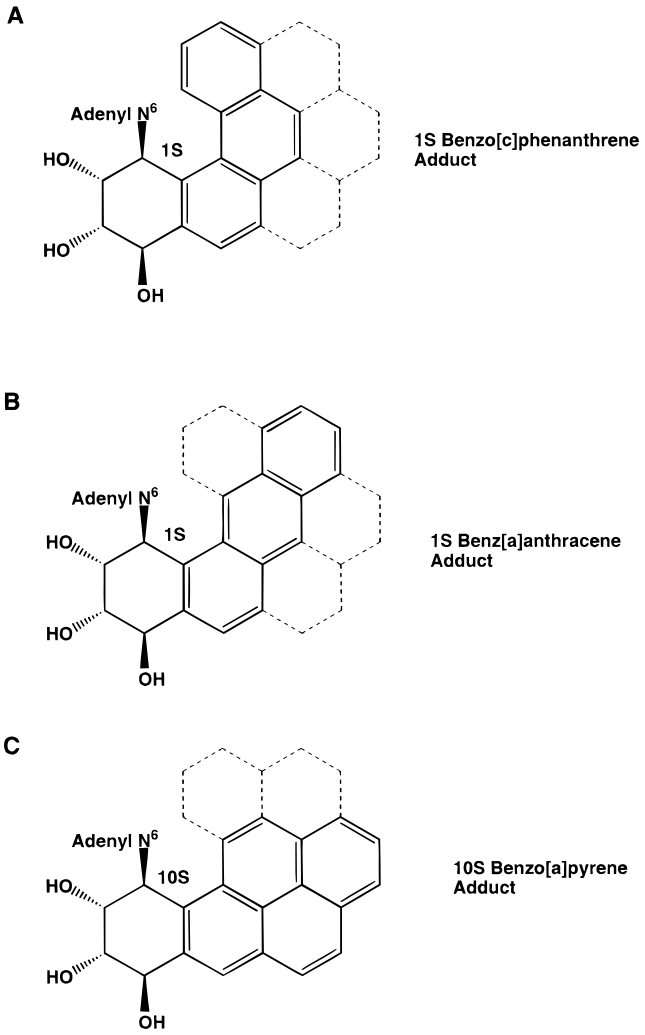

[a] When it is intercalated 3′ to the lesion site, we propose that the benzo[*c*]phenanthrene lesion is the least structurally perturbing to the B-DNA duplex. This adduct forms a stable structure (*41*). Likewise, the benz[*a*]anthracene adduct studied in this work also allows relatively facile intercalation of the pyrenyl moiety 3′ to the modified base pair. With the adenyl N^6 benzo[*a*]pyrene adduct (*26*), we propose that greater steric clash between the PAH ring and the complementary strand destabilizes the RSRS adduct.

opposite the incorrect partner, dG (*70*). In that instance, the modified adenine base rotated about the glycosyl bond χ to the syn conformation about χ. The effect of this rotation about χ was to provide the potential for formation of an A_{syn}·G_{anti} pairing. This perhaps compensated for the energetic penalty associated with insertion of the BP moiety 3′ to the lesion site.

The observation that the minor conformation observed in the work presented here involves rotation of $^{S,R,S,R}A^6$ into the syn conformation about the glycosyl bond is consistent with this model. Both the (1*S*)-BPh (*41*) and (1*S*)-BA adducts easily intercalate 3′ to the modified base pair when in the anti conformation about χ. In these instances, one would predict that for the modified adenine, the syn conformation about χ should be of higher energy, corresponding to the minor conformation. On the other hand, one might predict that incorrectly pairing either the (1*S*)-BPh or (1*S*)-BA adducts opposite dG should shift the equilibrium away from the anti conformation of χ. This might facilitate formation of an A_{syn}·G_{anti} pairing as observed for the (10*S*)-BP adduct opposite dG (*70*). It will be of interest to determine whether this prediction is borne out.

Structure−Function Relationships. Using a prokaryotic in vivo replication system, McNees et al. (*43*) showed that the BA SRSR(61,2) adduct is weakly mutagenic, producing low levels of A → G mutations. In all instances, the levels of mutations induced by the SRSR(61,2) adduct were substantially lower than those observed for the corresponding RSRS-(61,2) adduct with opposite stereochemistry at the benzylic carbon. For example, in repair-deficient (uvrA-, recA-) *E. coli* AB2480 cells, the SRSR(61,2) adduct yielded 0.3% A → G mutations, as compared to 2.6% A → G mutations for the RSRS(61,2) adduct. Thus, the stereospecific conformational difference exhibited by the SRSR(61,2) adduct as compared to the RSRS(61,2) adduct, in which the SRSR-(61,2) adduct is intercalated 3′ to the site of adduction, is reflected in the mutagenic outcome for this lesion. The results suggest the higher levels of A → G mutations induced in this replication system by the RSRS(61,2) lesion might be a consequence of specific conformational features related to the 5′-intercalation of the RSRS(61,2) adduct, which are not present in the 3′-intercalated SRSR(61,2) lesion. The SRSR-(61,2) adduct blocked DNA polymerase III to approximately the same degree as the BA RSRS(61,2) adduct in an in vitro polymerization assay (*43*). These replication blocks were conceivably induced by the intercalation of the SRSR(61,2) and RSRS(61,2) adducts into the DNA duplex, thus resulting in unwinding and structural distortion of the DNA.

The functional significance of the minor conformer of the SRSR(61,2) adduct, in which $^{S,R,S,R}A^6$ appears to be in the syn conformation about χ, is unclear. The population of the minor conformation (estimated from the NMR studies) was ∼20%, while the frequency of A → G mutations induced by the SRSR(61,2) adduct was ∼14−22% of that of the RSRS(61,2) adduct (*43*). This may be coincidental. The syn conformation of the modified $^{S,R,S,R}A^6$ represents a significant structural perturbation that may provide a rationale for a replication block and misreplication (*43*). As determined for the BP−(10*S*)-opposite dG adduct (*70*), a dG mismatch (as opposed to a dT match) opposite the BA−(1*S*)-dA adduct would allow formation of a A_{syn}·G_{anti} base pairing interaction. This would be predicted to generate A → C mutations. However, in the aforementioned in vivo mutagenesis studies (*43*), such mutations were not observed. One might conclude that mutations induced by the minor conformation do not involve transient formation of the A_{syn}·G_{anti} base pair. However, it should be emphasized that our understanding of structure−activity relationships for these adducts remains limited. A number of additional factors may play a role in modulating the biological processing of these adducts. For example, the exclusivity of A → G mutations at the SRSR-(61,2) site in the *ras61* sequence observed by Chary et al. (*71*) differed from the results of Page et al. (*72*), who examined the same adduct, but using a differing bacterial strain. In their experiments, A → T and A → C mutations were generated in addition to A → G mutations, which suggested the existence of strain-specific differences in the processing of these adducts.

Summary. The BA SRSR(61,2) adduct at adenine N^6 in the *ras61* coding sequence revealed the influence of stereochemistry upon adduct structure. Two conformations interchange around the glycosidic torsion angle of the modified adenine. In the major conformation, the anthracenyl moiety intercalated from the major groove to the 3′-side of the adduction. In the minor conformation, the syn conformation was observed.

ACKNOWLEDGMENT

We thank Mr. Markus Voehler for assistance with the collection of NMR data and Mr. Jason P. Weisenseel for assistance with processing the data. We also thank our reviewers for their helpful comments.

SUPPORTING INFORMATION AVAILABLE

Tables S1−S3, which detail the ^{1}H NMR chemical shift assignments; Table S4, which shows the experimental distances and classes of restraints; and Figure S1, which shows atomic charges obtained for the BA lesion. This material is available free of charge via the Internet at http://pubs.acs.org.

REFERENCES

1. Pott, P. (1963) *Natl. Cancer Inst. Monogr. 10*, 7−13.
2. Yang, S. K. (1988) *Biochem. Pharmacol. 37*, 61−70.
3. Guengerich, F. P., and Shimada, T. (1991) *Chem. Res. Toxicol. 4*, 391−407.
4. Dipple, A., Moschel, R. C., and Bigger, C. A. H. (1984) in *Chemical Carcinogens* (Searle, C. E., Ed.) pp 41−163, American Cancer Society, Washington, DC.
5. Geacintov, N. E. (1985) in *Polycyclic Hydrocarbons and Carcinogenesis* (Harvey, R. G., Ed.) pp 107−124, ACS Symposium Series, American Chemical Society, Washington, DC.
6. Thakker, D. R., Yagi, H., Levin, W., Wood, A. W., Conney, A. H., and Jerina, D. M. (1985) in *Bioactivation of Foreign Compounds* (Anders, M. W., Ed.) pp 177−242, Academic Press, New York.
7. Jennette, K. W., Jeffery, A. M., Blobstein, S. H., Beland, F. A., Harvey, R. G., and Weinstein, I. B. (1977) *Biochemistry 16*, 932−938.
8. Osborne, M. R., Jacobs, S., Harvey, R. G., and Brookes, P. (1981) *Carcinogenesis 2*, 553−558.
9. Grimmer, G. (1979) in *Environmental Carcinogens: Selected Methods of Analysis III*, International Agency for Research on Cancer, Lyon, France.
10. International Agency for Research on Cancer (1983) in *Monograph on the Evaluation of Carcinogenic Risk of the Chemical to Man: Certain Polycyclic Aromatic Hydrocarbons and Heterocyclic Compounds*, International Agency for Research on Cancer, Lyon, France.
11. Snook, M. E., Severson, R. F., Arrendale, R. F., Higman, H. C., and Chortyk, O. (1977) *Beitr. Tabakforsch. 9*, 79−101.
12. Levin, W., Chang, R. L., Wood, A. W., Yagi, H., Thakker, D. R., Jerina, D. M., and Conney, A. H. (1984) *Cancer Res. 44*, 929−933.
13. Slaga, T. J., Huberman, E., Selkirk, J. K., Harvey, R. G., and Bracken, W. M. (1978) *Cancer Res. 38*, 1699−1704.
14. Wood, A. W., Levin, W., Lu, A. Y., Ryan, D., West, S. B., Lehr, R. E., Schaefer-Ridder, M., Jerina, D. M., and Conney, A. H. (1976) *Biochem. Biophys. Res. Commun. 72*, 680−686.
15. Wood, A. W., Chang, R. L., Levin, W., Lehr, R. E., Schaefer-Ridder, M., Karle, J. M., Jerina, D. M., and Conney, A. H. (1977) *Proc. Natl. Acad. Sci. U.S.A. 74*, 2746−2750.
16. Harvey, R. G. (1982) *Am. Sci. 70*, 386−393.
17. Conney, A. H. (1982) *Cancer Res. 42*, 4875−4917.
18. Harvey, R. G. (1991) in *Polycyclic Aromatic Hydrocarbons: Chemistry and Carcinogeneicity*, Cambridge University Press, Cambridge, U.K.
19. Buening, M. K., Wislocki, P. G., Levin, W., Yagi, H., Thakker, D. R., Akagi, H., Jerina, D. M., and Conney, A. H. (1978) *Proc. Natl. Acad. Sci. U.S.A. 75*, 5358−5361.
20. Thakker, D. R., Levin, W., Yagi, H., Tada, M., Ryan, D. E., Thomas, P. E., Conney, A. H., and Jerina, D. M. (1982) *J. Biol. Chem. 257*, 5103−5110.
21. MacNicoll, A. D., Cooper, C. S., Ribeiro, O., Pal, K., Hewer, A., Grover, P. L., and Sims, P. (1981) *Cancer Lett. 11*, 243−249.
22. Feng, B., and Stone, M. P. (1995) *Chem. Res. Toxicol. 8*, 821−832.
23. Feng, B., Voehler, M. W., Zhou, L., Passarelli, M., Harris, C. M., Harris, T. M., and Stone, M. P. (1996) *Biochemistry 35*, 7316−7329.
24. Feng, B., Zhou, L., Passarelli, M., Harris, C. M., Harris, T. M., and Stone, M. P. (1995) *Biochemistry 34*, 14021−14036.
25. Stone, M. P., and Feng, B. (1996) *Magn. Reson. Chem. 34*, S105−S114.
26. Zegar, I. S., Kim, S. J., Johansen, T. N., Horton, P., Harris, C. M., Harris, T. M., and Stone, M. P. (1996) *Biochemistry 35*, 6212−6224.
27. Li, Z., Mao, H., Kim, H. Y., Tamura, P. J., Harris, C. M., Harris, T. M., and Stone, M. P. (1999) *Biochemistry 38*, 2969−2981.
28. Barbacid, M. (1987) *Annu. Rev. Biochem. 56*, 779−827.
29. Harris, C. M., Zhou, L., Strand, E. A., and Harris, T. M. (1991) *J. Am. Chem. Soc. 113*, 4328−4329.
30. Kim, S. J., Harris, C. M., Koreeda, M., and Harris, T. M. (1991) *Tetrahedron Lett. 32*, 6073−6076.
31. Kim, S. J., Stone, M. P., Harris, C. M., and Harris, T. M. (1992) *J. Am. Chem. Soc. 114*, 5480−5481.
32. Kim, S. J., Jajoo, H. K., Kim, H.-Y., Zhou, L., Horton, P., Harris, C. M., and Harris, T. M. (1995) *Bioorg. Chem. 3*, 811−822.
33. Dipple, A., Pigott, M., Moschel, R. C., and Costantino, N. (1983) *Cancer Res. 43*, 4132−4135.
34. Vousden, K. H., Bos, J. L., Marshall, C. J., and Phillips, D. H. (1986) *Proc. Natl. Acad. Sci. U.S.A. 83*, 1222−1226.
35. Ralston, S. L., Seidel, A., Luch, A., Platt, K. L., and Baird, W. M. (1995) *Carcinogenesis 16*, 2899−2907.
36. Schurter, E. J., Yeh, H. J. C., Sayer, J. M., Lakshman, M. K., Yagi, H., Jerina, D. M., and Gorenstein, D. G. (1995) *Biochemistry 34*, 1364−1375.
37. Yeh, H. J. C., Sayer, J. M., Liu, X., Altieri, A. S., Byrd, R. A., Lakshman, M. K., Yagi, H., Schurter, E. J., Gorenstein, D. G., and Jerina, D. M. (1995) *Biochemistry 34*, 13570−13581.
38. Schwartz, J. L., Rice, J. S., Luxon, B. A., Sayer, J. M., Xie, G., Yeh, H. J., Liu, X., Jerina, D. M., and Gorenstein, D. G. (1997) *Biochemistry 36*, 11069−11076.
39. Schurter, E. J., Sayer, J. M., Oh-hara, T., Yeh, H. J. C., Yagi, H., Luxon, B. A., Jerina, D. M., and Gorenstein, D. G. (1995) *Biochemistry 34*, 9009−9020.
40. Cosman, M., Fiala, R., Hingerty, B. E., Laryea, A., Lee, H., Harvey, R. G., Amin, S., Geacintov, N. E., Broyde, S., and Patel, D. (1993) *Biochemistry 32*, 2488−2497.
41. Cosman, M., Laryea, A., Fiala, R., Hingerty, B. E., Amin, S., Geacintov, N. E., Broyde, S., and Patel, D. J. (1995) *Biochemistry 34*, 1295−1307.
42. Geacintov, N. E., Cosman, M., Hingerty, B. E., Amin, S., Broyde, S., and Patel, D. J. (1997) *Chem. Res. Toxicol. 10*, 111−146.
43. McNees, A. G., O'Donnell, M., Horton, P. H., Kim, H. Y., Kim, S. J., Harris, C. M., Harris, T. M., and Lloyd, R. S. (1997) *J. Biol. Chem. 272*, 33211−33219.
44. Millican, T. A., Mock, G. A., Chauncey, M. A., Patel, T. P., Eaton, M. A. W., Gunning, J., Cutbush, S. D., Neidle, S., and Mann, J. (1984) *Nucleic Acids Res. 12*, 7435−7453.
45. Schmitz, U., and James, T. L. (1995) *Methods Enzymol. 261*, 3−44.

46. Allain, F. H., and Varani, G. (1995) *J. Mol. Biol. 250*, 333−353.
47. Borer, P. N. (1975) in *Handbook of Biochemistry and Molecular Biology*, CRC Press, Cleveland, OH.
48. Piotto, M., Saudek, V., and Sklenar, V. (1992) *J. Mol. Biol. 6*, 661−665.
49. Keepers, J. W., and James, T. L. (1984) *J. Magn. Reson. 57*, 404−426.
50. Borgias, B. A., and James, T. L. (1990) *J. Magn. Reson. 87*, 475−487.
51. Liu, H., Tonelli, M., and James, T. L. (1996) *J. Magn. Reson., Ser. B 111*, 85−89.
52. Rinkel, L. J., and Altona, C. (1987) *J. Biomol. Struct. Dyn. 4*, 621−649.
53. Nikonowicz, E. P., and Gorenstein, D. G. (1990) *Biochemistry 29*, 8845−8858.
54. Saenger, W. (1984) in *Principles of Nucleic Acid Structure*, Springer, New York.
55. Weisz, K., Shafer, R. H., Egan, W., and James, T. L. (1994) *Biochemistry 33*, 354−366.
56. Tonelli, M., Ragg, E., Bianucci, A. M., Lesiak, K., and James, T. L. (1998) *Biochemistry 37*, 11745−11761.
57. Brunger, A. T. (1992) in *X-Plor. Version 3.1. A system for X-ray Crystallography and NMR*, Yale University Press, New Haven, CT.
58. Nilsson, L., Clore, G. M., Gronenborn, A. M., Brunger, A. T., and Karplus, M. (1986) *J. Mol. Biol. 188*, 455−475.
59. Ravishankar, G., Swaminathan, S., Beveridge, D. L., Lavery, R., and Sklenar, H. (1989) *J. Biomol. Struct. Dyn. 6*, 669−699.
60. Nilges, M., Clore, G. M., and Gronenborn, A. M. (1988) *FEBS Lett. 239*, 129−136.
61. Wimberly, B. T. (1992) Ph.D. Dissertation, University of California, Berkeley, CA.
62. Wimberly, B., Varani, G., and Tinoco, I., Jr. (1993) *Biochemistry 32*, 1078−1087.
63. Boelens, R., Scheek, R. M., Dijkstra, K., and Kaptein, R. (1985) *J. Magn. Reson. 62*, 378−386.
64. Allain, F. H., and Varani, G. (1997) *J. Mol. Biol. 267*, 338−351.
65. Mauffret, O., Amir-Aslani, A., Maroun, R. G., Monnot, M., Lescot, E., and Fermandjian, S. (1998) *J. Mol. Biol. 283*, 643−655.
66. Zegar, I. S., Chary, P., Jabil, R. J., Tamura, P. J., Johansen, T. N., Lloyd, R. S., Harris, C. M., Harris, T. M., and Stone, M. P. (1998) *Biochemistry 37*, 16516−16528.
67. Feigon, J., Wang, A. H. J., Van Der Marel, G. A., Van Boom, J. H., and Rich, A. (1984) *Nucleic Acids Res. 12*, 1243−1263.
68. Cosman, M., Fiala, R., Hingerty, B. E., Laryea, A., Lee, H., Harvey, R. G., Amin, S., Geacintov, N. E., Broyde, S., and Patel, D. (1993) *Biochemistry 32*, 2488−2497.
69. Cosman, M., Laryea, A., Fiala, R., Hingerty, B. E., Amin, S., Geacintov, N. E., Broyde, S., and Patel, D. J. (1995) *Biochemistry 34*, 1295−1307.
70. Yeh, H. J. C., Sayer, J. M., Liu, X., Altieri, A. S., Byrd, R. A., Lakshman, M. K., Yagi, H., Schurter, E. J., Gorenstein, D. G., and Jerina, D. M. (1995) *Biochemistry 34*, 13570−13581.
71. Chary, P., Latham, G. J., Robberson, D. L., Kim, S. J., Han, S., Harris, C. M., Harris, T. M., and Lloyd, R. S. (1995) *J. Biol. Chem. 270*, 4990−5000.
72. Page, J. E., Zajc, B., Oh-hara, T., Lakshman, M. K., Sayer, J. M., Jerina, D. M., and Dipple, A. (1998) *Biochemistry 37*, 9127−9137.

BI9903650